Applied Catalysis B: Environmental 304 (2022) 120984

Contents lists available at ScienceDirect

Applied Catalysis B: Environmental

journal homepage: www.elsevier.com/locate/apcatb

Ethanol to distillate-range molecules using Cu/Mg_xAlO_y catalysts with low Cu loadings

Paolo A. Cuello-Penaloza [a], Raka G. Dastidar [a], Shao-Chun Wang [b], Yi Du [c], Michael P. Lanci [c], Bradley Wooler [c], Christine E. Kliewer [c], Ive Hermans [b], James A. Dumesic [a], George W. Huber [a,*]

[a] Department of Chemical and Biological Engineering, University of Wisconsin, 1415 Engineering Drive, Madison, WI 53706, United States
[b] Department of Chemistry, University of Wisconsin-Madison, 1101 University Ave, Madison, WI 53706, United States
[c] ExxonMobil Research and Engineering, 3545 Route 22 East Clinton Township, Annandale, NJ 08801, United States

ARTICLE INFO

Keywords:
Alcohol coupling reactions
Esterification
Mixed metal oxides
Schultz-Flory distribution
Catalyst stability

ABSTRACT

A series of calcined MgAl mixed metal oxide catalysts with low Cu loadings (0.1–1.5 wt%) were tested for ethanol oligomerization to distillate-range molecules. The low Cu loading catalysts (0.1–0.6 wt%) had high selectivity to linear chain C_{4+} alcohols (49–63% selectivity) and C_{6+} esters (45–66% of total esters). More specifically, the diesel fuel precursor selectivities were over 75% for low Cu loading catalysts (0.1–0.6 wt%), with a decrease to 49% for a higher Cu loading catalyst (>1.2 wt% Cu) due to increased ethyl acetate and acetone formation. Alcohol and ester product selectivities follow a Schultz-Flory distribution. Alcohol selectivity was found to vary inversely with BET surface areas of the catalysts, whereas ester selectivity was found to increase with higher base site counts. However, Cu wt% loading was found to have a stronger impact in overall catalyst activity. The catalysts deactivated proportionally to the number of turnovers mainly due to coking, but could be regenerated by calcination.

1. Introduction

The production of C_8-C_{22} distillate-range fuels has been a topic of increasing importance in the last few decades. In the next 20 years, an increase in demand for heavy-duty fuels is projected [1], with a concomitant decrease in demand for light duty fuels, such as gasoline. Moreover, there is a strong drive to produce fuels with lower greenhouse gas (GHG) emissions [2,3]. The most commonly produced low carbon liquid fuel is ethanol which has been reported to have 39–108% reduction in GHG emissions compared to gasoline, depending on the biomass source it is produced from, and also on the ethanol production technology [4,5]. Several approaches have been proposed to convert ethanol into diesel, none of which are commercially practiced today [3]. Our group has previously proposed a route to convert ethanol into distillate-range fuel molecules by a two-step approach that involves Guerbet coupling of ethanol to longer alcohols and subsequent acid-catalyzed etherification of the alcohols [6]. The ethers produced have properties that are similar to diesel fuels [7]. The key challenge of the Guerbet step is to selectively oligomerize the alcohols into C_{4+} primary linear alcohols in high yields, which can then undergo etherification. Branched alcohols produce olefins as major products during the acid catalyzed etherification step.

One of the most researched catalysts for the production of 1-butanol and higher alcohols from ethanol are stoichiometric hydroxyapatites (HAP) of Ca and Sr [8,9]. HAPs are particularly selective to 1-butanol (>70% at <15% conversion) and higher alcohols due to its good balance of acid and base sites [10]. Moteki and Flaherty [11] have previously studied ethanol conversion over Ca and Sr-HAP catalysts and proposed a series of relevant kinetic steps to describe this reaction proceeding via aldol condensation. They found that the linear-to-branched ratio of C_6 alcohols was found to be a weak function of temperature, always being slightly lower than 1; and more importantly, that selectivities to alcohols and aldehydes decreased with conversion and could be described by a modified step-growth model. However, our group [6] demonstrated that chain growth with Ca-HAP is limited for the Guerbet coupling of ethanol after 50% conversion because branched alcohols are essentially inactive as nucleophiles in the Guerbet coupling reaction [12], tending instead to undergo dehydration to form olefins. Moreover, selectivity to dehydration products also increases with concomitant decrease of selectivity to coupling products

* Corresponding author.
E-mail address: gwhuber@wisc.edu (G.W. Huber).

https://doi.org/10.1016/j.apcatb.2021.120984
Received 24 July 2021; Received in revised form 20 October 2021; Accepted 28 November 2021
Available online 3 December 2021

due to water inhibition [12] affecting more severely the latter reactions, as also reported by Hanspal et al. [10] Our group also proposed a kinetic model for the Guerbet coupling of ethanol and several dehydration side reactions using Ca-HAP[12], which was capable of accurately predicting conversion and product selectivities in all conversion ranges. According to the kinetic model, a good catalyst for alcohol coupling must either favor increased events of ethanol attacking other alcohols (higher nucleophilicity of ethanol relative to that of higher alcohols) or decreased events of higher alcohols attacking ethanol (lower electrophilicity of ethanol relative to that of higher alcohols) to produce larger linear chain alcohols capable of undergoing subsequent coupling reactions. The C_{6+} primary branched alcohols produced by Guerbet coupling are highly selective (>80%) to olefins in the acid catalyzed etherification step of alcohols to ethers [6] and the linear-to-branched chain alcohol ratios of C_6 molecules was only 0.8 for HAP, which is consistent with Moteki and Flaherty findings and also was found to decrease as the alcohols increase in molecular weight. Consequently, these factors limit both the ability of HAP to produce increasingly larger alcohols as conversion increases, and the suitability of the produced alcohols for upgrading by acid-catalyzed etherification as branching is significant and more of it will occur the higher the conversion is.

A handful of other catalysts have been studied for ethanol oligomerization. These include base metals such as Cu or Ni supported on Mg_xAlO_y mixed metal oxides derived from calcination of layered double hydroxides (LDH)[13]. The performance of these catalysts varies depending on the reaction conditions and the nature of the catalysts. Marcu et al.[14] used Cu/Mg_xAlO_y catalysts with 1.1–22.9 wt% Cu loadings for Guerbet coupling of ethanol using batch reactors at 200 °C, obtaining 1-butanol selectivity up to 50% at low conversion. Bravo-Suarez et al. [15] used methanol/ethanol mixtures in a flow reactor and observed low selectivities to alcohols (5–10%) but higher selectivities to esters(~50%). Cheng et al. [16] tested Mg_xAlO_y doped with 1 wt% Cu in the coupling of methanol/ethanol mixtures, varying the Mg/Al ratio from 1 to 5. They found that the conversion rates and space-time yields of C_{3+} products increased with the exposed Cu^0 area, which in turn was affected non-monotonically by the Mg/Al ratio. A particular approach to tune Cu/Mg_xAlO_y catalysts to be more selective to higher alcohols in the ethanol oligomerization reaction was proposed by Ramasamy and coworkers [17–19] The researchers observed that catalysts with $\leq$0.1 wt% Cu were able to catalyze the conversion of ethanol to 1-butanol and higher alcohols with selectivities up to 75%, while side-reactions such as esterification and ketone formation were suppressed. They proposed that at very low Cu loadings the active site is Cu^{+1}, not metallic Cu, as indicated from *in-situ* XANES and EXAFS. However, no articles have been published about this approach applied to alcohol coupling as of present, and no mention of the branching patterns of the product alcohols is reported in any literature.

Numerous methods are available in literature to synthesize well-defined mixed metal oxide catalysts (particularly MgAl) by co-precipitation [20,21]. It is possible to vary the surface area and porosity of the LDH precursor by changing process parameters, including pH of titration, temperature, and organic solvent washing (acetone/ methanol) [22,23]. It is also possible to synthesize materials with varying M^{+2}/M^{+3} ratios (where M is the metal and +2/+3 are the valences) to promote desired base or acid-catalyzed reactions [24–26]. The solid phase composition of the resulting material differs with the metal function ratios. For instance, in the case of MgAl mixed oxides it is possible to obtain a homogeneous MgO-like structure active in alcohol dehydrogenation reactions if Mg/Al > 1 [24]. For lower Mg/Al ratios, combined $MgAl_2O_4$, MgO and Al_2O_3 heterogeneous phases may be obtained, and the performance of the resulting catalyst will increasingly lean towards acid-catalyzed reactions such as dehydrations. When a metal function such as Cu is added, the resulting material properties such as base site counts and reduction profile will change, having an impact on the performance of reactions such as dehydrogenations or dehydration of alcohols and coupling of alcohols and aldehydes[15,16]. Therefore, LDH catalysts can be flexibly synthesized and the variation of the resulting properties of the materials may be studied in regards any reaction by employing co-precipitation synthesis techniques. Finally, calcination temperatures can also impact the performance of these catalysts in ethanol condensation reactions, as this parameter can affect the relative amounts of acid-to-base sites as well as the bulk structure and cation environment of the metals as argued by Ramasamy et al. [21] who found that for ethanol condensation the best calcination temperature of MgAl LDH to obtain higher C-number products was 600 °C.

The objective of this paper is to study ethanol oligomerization to diesel fuel precursors over low Cu loading catalysts supported on high surface area LDH-derived MgAl mixed oxides. Diesel fuel precursors (DFP) are defined as any alcohol, aldehyde or ketone with 4 or more carbon atoms, or any ester, ether, hemiacetal or acetal with more than 6 carbon atoms, as these species are either in the distillate-range (C_{10+} sizes) or can ultimately be upgraded via acid catalysis to higher molecular weight ethers (bimolecular dehydration) or esters (transesterification). As we will show in this paper, these catalysts produce linear alcohols, esters and other diesel fuel precursors from ethanol at high selectivity.

2. Experimental section

2.1. Catalyst synthesis

Synthesis of materials was done by co-precipitation techniques carried out by our group in other research [27], with the use of solvents (acetone, methanol)[22], or by incipient wetness impregnation. The materials were labeled as wtCuMMO(d), where 'wt' is the Cu wt% nominal loading, and d is a description of the catalyst depending on the BET surface area (vl = very low, l = low, m = medium, h =high), the method of preparation (i – incipient wetness impregnation), a physical mixture (pm), and a regenerated catalyst(r). Target materials prepared were: 0CuMMO, 0.1CuMMO, 0.3CuMMO(vl), 0.3CuMMO(l), 0.3CuMMO(m), 0.3CuMMO(h), 0.3CuMMO(i) and 1.2CuMMO.

Three aqueous solutions were prepared: solution 1 contains aqueous solutions of $Mg(NO_3)_2.6(H_2O)$ (Sigma-Aldrich 237175), $Al(NO_3)3{\cdot}9(H_2O)$ (Sigma-Aldrich 237973), and $Cu(NO_3)_2.3(H_2O)$ (Sigma-Aldrich 61194) in appropriate amounts, solution 2 is a 0.133 M (for 0.1CuMMO) or 0.512 M aqueous Na_2CO_3 (Sigma-Aldrich 223530) solution, and solution 3 contains a 1 M (for 0.1CuMMO) or 50 wt% NaOH (Sigma-Aldrich 795429) aqueous solution. The Na_2CO_3 solution was added to a 1 L beaker and either heated to 60 °C (for 0.1CuMMO) or maintained at room temperature and stirred with a magnetic stir bar. Solution 1 containing Cu, Mg and Al metals and solution 3 containing NaOH were slowly added to the 1 L beaker using a syringe pump. The flow rates of solution 1 and 3 were controlled so that addition would take place over 1 h and so the pH was maintained at 10 (or 11 for 0.1CuMMO) during the addition. A temperature/pH probe (Ohaus ST20) was used to monitor the pH and temperature of the solution. After all solutions were added, the mixed solution was aged differently depending on the catalyst. For 0.1CuMMO, the aging was done for 20 h in a 1 L bottle at 60 °C with stirring, for 0.3CuMMO(vl) and 0.3CuMMO(l) catalyst, aging was done at 60 °C for 12 h, for all other catalysts aging was done at room temperature for 24 h. After the aging process, the mixed solution was washed and filtered to remove residual nitrates and sodium. The filter cake was dissolved in 300 mL of 1 M Na_2CO_3 solution and then washed with 500 mL of DI water and filtered. The filter cake was dissolved in 500 mL of DI water and washed and filtered 2 more times for 0.1CuMMO and for 0.3CuMMO(vl) (due to having more residual Na content to be removed than other materials). For all other materials, washing was done with water and acetone, and for 0.3CuMMO(h) the resultant gel was redispersed in 1 L of acetone at 60 °C for 2 h after washing. The filter cakes were dried overnight in a 110 °C oven or in a vacuum oven at room temperature (0.3CuMMO(h)). The dry catalysts were then crushed and calcined at 600 °C for 2 h on a 4 °C/min temperature ramp. The catalyst

is then sieved to 30 – 80 mesh and packed into the reactor where it is reduced *in situ* at 325 °C for 12 h with a 4 °C/min temperature ramp under 50 mL/min H_2 flow before the start of any run.

For the 0.3CuMMO(i) catalyst, Cu addition was done using incipient wetness impregnation by dropwise addition of $Cu(NO_3)_2.3(H_2O)$ (Sigma-Aldrich 61194) aqueous solution to MgAl hydrotalcite (Sigma-Aldrich 652288), then drying, calcining and reducing the catalyst as described in the previous paragraph. A physical mixture of 0CuMMO catalyst (no Cu content) with 1.2CuMMO catalyst was prepared by mixing 0.9213 ± 0.0001 g of the undoped material with $0.0832\ g \pm 0.0001$ g of 1.2CuMMO. This mixture was labeled 0.1CuMMO(pm).

2.2. Ethanol oligomerization reactions

Ethanol oligomerization reactions were performed in stainless-steel fixed-bed reactors (40 cm long, 2.54 cm catalyst bed, 0.95 cm outer diameter) and analyzed using the scheme described next (and first elsewhere [6]). The reactors were packed with 1 g of CuMMO catalysts pelletized and sieved to a particle size of 250–354 μm. Prior to reaction, the catalysts were reduced *in situ* as described in the previous section. Ethanol was fed with a syringe pump (Teledyne ISCO) at 21–139 μL min^{-1}, with H_2 cofeed at 2–50 mL/min in the downflow configuration at atmospheric pressure through a preheated evaporation region maintained at > 200 °C prior to entering the reactor, ensuring that the feed is completely in the gas phase before contacting the catalyst. The gas composition entering the reactor was 80 mol% ethanol and 20 mol% H_2.

The reactor was heated with a tube furnace (Lindberg Blue M Mini-Mite) with the temperature kept uniform via an aluminum block (30 cm long) positioned between the reactor and furnace coils [6]. Below the furnace, the products were kept heated at > 150 °C prior to passing through a removable 110 mL glass condenser (Ace Glass). Gases which did not condense were sent to a three-way valve positioned to flow either through a bubble-flow meter and then to vent or to an online gas GC (Shimadzu 2010) equipped with a flame ionization detector (FID) and a thermal conductivity detector (TCD). The FID line utilized a Rt-Q-BOND column (Restek), while the TCD line utilized a Hayesep D column (Supelco). Negligible permanent gases were detected via the TCD, thus this line was not used for quantification. Gas and liquid samples were collected simultaneously every 0.8–5.5 h (typically every 1.25 h). Gas samples were first injected into the GC via a six-way valve, after which the gas flow rate was measured via the bubble flow meter. The outlet flow from the reactor was redirected from the product collection condenser to a waste condenser on the side where the liquid would drop and the gas flow would emerge and be redirected to vent, then the ice bath was lowered in order for the condenser containing the collected product to be removed and immediately replaced with another, after which the outlet flow would finally be redirected from the waste condenser to the new product collection condenser. To reduce sampling error caused by transient vapor–liquid equilibria and low product volumes, 5 – 20 mL of 1-propanol was generally added to the condenser prior to collection. After collection, the sample mass was weighed, and the liquid was diluted with 1-propanol including a known amount of 1-pentanol as an internal standard. The products were then analyzed and quantified via GC-FID (Shimadzu 2014) equipped with a RTX-VMS column (Restek). Products were quantified with GC-FID via external standards when reference compounds could be obtained. When they could not, response factors were estimated via the effective carbon number method. Products were identified via external standards when available, or via GC-MS suggestions.

Yield of each species was calculated using the following formula:

$$Y_i = \frac{n_{C,i,out}}{n_{C,in}} \tag{1}$$

Conversion was calculated using the following formula:

$$X = \sum_{i=1}^{n} Y_i \tag{2}$$

Selectivity was calculated in product yield-basis using this formula:

$$S_i = \frac{Y_i}{\sum_{i=1}^{n} Y_i} = \frac{Y_i}{X} \tag{3}$$

Diesel fuel precursors (DFP) are defined as any alcohol, aldehyde or ketone with 4 or more carbon atoms, or any ester, ether, hemiacetal or acetal with more than 6 carbon atoms. Diesel fuel precursor selectivity (DFPS) is then defined as:

$$DFPS = \sum_{i=1}^{n} S_{C4+alcohols} + \sum_{i=1}^{n} S_{C4+aldehydes} + \sum_{i=1}^{n} S_{C4+ketones} + \sum_{i=1}^{n} S_{C6+esters} \sum_{i=1}^{n} S_{C6+ethers} + \sum_{i=1}^{n} S_{C6+hemiacetals} + \sum_{i=1}^{n} S_{C6+acetals} \tag{4}$$

Another feature investigated in this work is the selectivity distribution of alcohols and esters according to the Schultz-Flory model [28,29]. This model is defined by the following equation:

$$ln\left(\frac{\boldsymbol{C_n}}{\boldsymbol{n}}\right) = (\boldsymbol{n}-\boldsymbol{1})ln(\boldsymbol{\alpha}) + \boldsymbol{2}ln(\boldsymbol{1}-\boldsymbol{\alpha}) \tag{5}$$

Where n is repeat unit defined as ethanol, C_n is carbon selectivity of alcohol (or ester) with n-repeat units, α is the chain-growth probability which in this case is the probability of an adsorbed C_n alcohol chain to grow to C_{n+1} (e.g. increase of n from 1 to 2 represents growth from ethanol to 1-butanol), and (1-α) is the desorption probability which in this case is the probability of obtaining a C_n alcohol product [29]. The α parameter is then calculated from the slope of an $ln(C_n/n)$ vs n plot.

We also studied catalyst deactivation with time on stream (TOS) at different WHSV. In Eq. (6), x(t) is conversion at TOS and $x_{0,WHSVi}$ is the initial conversion at the ith WHSV. We plotted the catalyst activity (a), as defined in Eq. (6) against the number of turnovers for the catalyst. A linear relationship between the two quantities was obtained as shown in Fig. 9.

$$\frac{x(t)}{x_{0,WHSV_i}} = a \tag{6}$$

Finally, we also performed a regeneration procedure to one of the catalysts by calcining it at 450 °C for 4 h with a 1 °C/min ramp, then reducing it again at typical reaction conditions.

2.3. Catalyst characterization

CuMMO catalysts textural properties were determined via N_2 physisorption using a Micromeritics ASAP 2020 instrument. Properties obtained were BET surface area, BJH pore size distribution and pore volume. The catalysts acid and base sites were determined via NH_3-TPD and CO_2-TPD respectively using modified methods reported in literature [25,26]. For this, a Micromeritics 2720 II equipment was used. Samples were pre-reduced at 350 °C before being treated with 25 mL of NH_3 or CO_2. The temperature range of the analyses were 150 – 600 °C for NH_3-TPD and 50 – 600 °C for CO_2-TPD. Actual compositions of Mg, Al and Cu of the catalysts were obtained by ICP-OES (Varian Vista-MPX) after digesting 10–15 mg of the solid samples in 10 mL of 10 wt% HNO_3 (trace metal grade, Sigma-Aldrich no. 438073) aqueous solution and diluting the digestate to 1 wt% HNO_3. Calibration curves of the metals were prepared from 1000 ppm standard solutions of Cu (Fluka – 68921), Mg (Ricca – RV010077) and Al (Fluka – 61935).

Powder X-ray diffraction of the catalyst samples was carried out in Rigaku Rapid II diffractometer. A Mo Kα source (λ = 0.71 Å) was used for the measurements and the scanned zone was 2θ = 5–60°. All measurements were recalculated to Cu Kα source (λ = 1.54 Å) for ease of

Table 1
Properties of the synthesized catalysts.

Catalyst	0.3CuMMO (vl)	0.3CuMMO (l)	0.3CuMMO (m)	0.3CuMMO (h)	0.3CuMMO (i)	0.1CuMMO	1.2CuMMO	0CuMMO
Actual Cu wt%[a,b]	0.4	0.3	0.3	0.4	0.6	0.2	1.5	0
Cu:Al[a]	0.01	0.009	0.008	0.009	0.02	0.006	0.04	0
Mg:Al[a]	2.8	3.0	2.9	2.8	3.0	3.3	2.8	2.9
LDH BET surface area (m^2/g)	82	98	250	382	388	–	235	388
Calcined LDH BET surface area (m^2/g)	148	129	172	192	176	187	208	268
Pore Volume (cm^3/g)	0.3	0.5	0.5	0.9	0.6	0.3	0.9	1.2
Base sites (μmol/g)	209	263	325	549	332	215	512	327
Acid sites (μmol/g)	1698	589	861	788	401	751	535	818

[a] Elemental composition of the catalysts from ICP-OES.
[b] Calculated Cu wt% loading is based on a fully decomposed hydrotalcite at the obtained Cu:Mg:Al ratio.

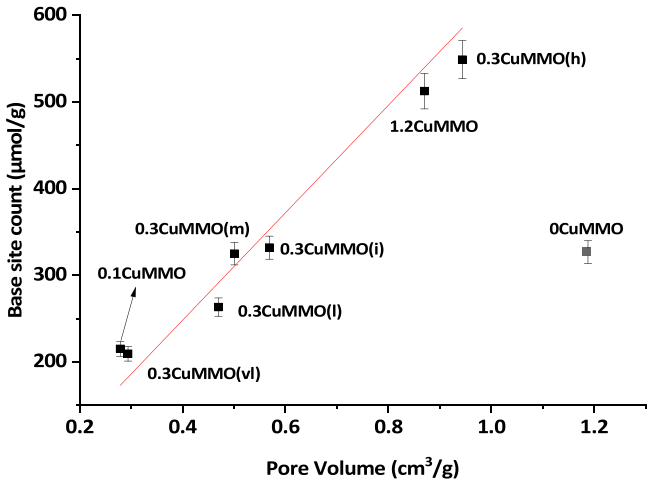

Fig. 1. Base site vs pore volume correlation for Cu/Mg_xAlO_y catalysts. Red line is linear fit of base site counts vs pore volume, Pearson's r = 0.9943; Adjusted R^2 = 0.9867, 0CuMMO catalyst (shown in translucent black) is left out of the correlation.

analysis and comparison with literature. Structures were matched with the use of JADE, PDF 4 + software, as well as from reports in literature. Thermogravimetric analysis was carried out using a TGA TA Q500. For analysis, 10 – 15 mg of sample were added to the dish and heated up from room temperature to 650 °C at a 10 °C/min ramp under oxygen flow. Total organic carbon (TOC) analysis of the fresh calcined and spent 0.1CuMMO and 0.3CuMMO(m) catalysts were made with a Shimadzu TOC-V CPH/CPN using the SSM-5000A solid sample module under a 100 mL/min O_2 flow. The instrument was calibrated with potassium phthalate (Sigma-Aldrich P1088) from 0 to 80 mg, and 48–62 mg of sample were weighed for the analysis. For TEM, the catalyst powder was prepared for characterization by crushing it into small pieces (<100 nm thick) using an agate mortar and pestle. The fines were dusted onto a 200 mesh, holey-carbon-coated, copper TEM grid. The grid was examined in the bright field (BF) TEM imaging mode of a Philips CM200F electron microscope that was operated at an accelerating voltage of 200 kV. Digital images were collected from randomly selected areas using a Gatan CCD camera and Digital Micrograph v. 2.5.4 software.

Fourier Transform Infrared Spectroscopy (FT-IR) was done to some of the samples after dosing CO in order to determine the nature of Cu sites on the catalytic surface. In order to make measurements comparable between samples, 5 ± 0.1 mg of these were weighed before they were pelletized under 2 ton of pressure for 30 s. The sample pellets are heated under 40 mL/min 4%H_2/N_2 flow to 325 °C with 4 °C/min ramp and held for 5 min, then cooled down to room temperature while maintaining %H_2/N_2 flow. When cooling down to room temperature, the cell was evacuated to 10^{-6} hPa, and then liquid nitrogen was used to further cool down to −150 °C with background scan. CO adsorption FT-IR (Bruker Vertex 70) spectra are collected after dosing 60 Torr 5%CO/He for 5 min. Finally, the CO is evacuated from the system, and another spectra is then collected after 9 min.

Table 2
Diesel fuel precursor compounds selectivity (DFPS), C_{4+} alcohol and aldehyde selectivities, C_{6+} ester selectivity and acetaldehyde, ethyl acetate and 1-ethoxyethanol selectivities for CuMMO catalyst formulations.

Catalyst (wt%CuMMO (d))[a]	0.3 (vl)	0.3 (l)	0.3 (m)	0.3 (h)	0.3 (i)	1.2	0.1	0.1 (r)	0.1 (pm)[b]
Conversion (%)[c]	49	51	54	54	43	44	45	47	39
DFPS (%)	75	81	75	77	75	49	79	78	84
C_6 L:B[d]	3.4	3.3	3.5	3.3	3.7	3.0	3.2	3.1	3.7
C_{4+} Alcohols (%)	55	57	50	49	51	27	56	54	63
C_{4+} Aldehydes (%)	10	11	11	9	10	6	11	10	13
C_{6+} Esters (%)	5	11	12	15	10	11	9	10	6
Others[e] **(%)**	30	21	27	27	29	56	24	26	18
Acetaldehyde (%)	4	3	4	5	7	5	6	5	6
Ethyl acetate (%)	3	9	9	10	13	30	9	7	3
1-ethoxyethanol (%)	2	1	1	1	1	1	2	1	2
α-Alcohols[f]	0.210	0.182	0.162	0.21	0.147	0.050	0.158	0.186	0.26
α-Esters[f]	0.43	0.32	0.30	0.39	0.21	0.19	0.29	0.33	0.21

Conditions: 325 °C, 300 psi, 6.56 h^{-1}
[a] Labels only contain Cu wt% and descriptor (d) if any, as all materials are CuMMO.
[b] This experiment is a physical mixture of 1.2CuMMO and 0CuMMO that has a total nominal Cu wt% of 0.1%.
[c] Conversion is defined as average of data points before 5000 turnovers on total Cu content basis of each catalyst by ICP-OES. Data typically is taken in the first 2500 turnovers.
[d] C_6 L:B = linear to branched C6 alcohol ratio.
[e] Others include Acetaldehyde, ethyl acetate, ethers, ketones, paraffins, olefins, hemiacetals and acetals (Refer to Tables S1–S9).
[f] These are the propagation probability (α-values) calculated from the Schultz-Flory distribution (Eq. (5)).

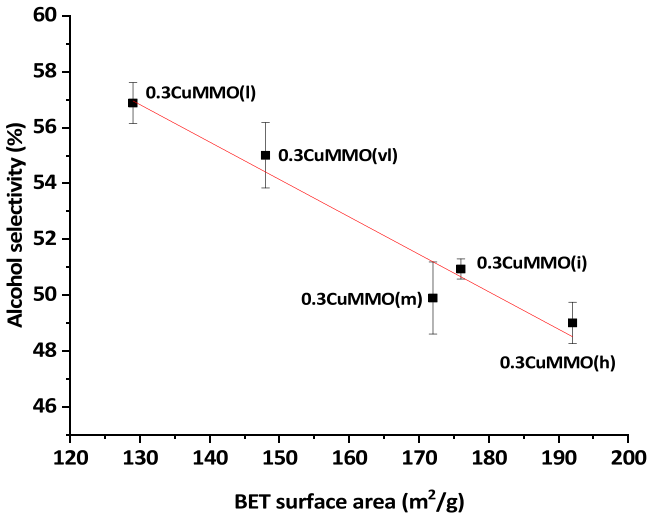

Fig. 2. Alcohol selectivity vs BET surface area in 0.3 wt%Cu (nominal) CuMMO catalysts. Conditions as described in Table 2. Red line is linear fit of alcohol selectivity vs BET surface area. Pearson's r = - 0.9744, Adjusted R^2 = 0.9325. (For interpretation of the references to colour in this figure, the reader is referred to the web version of this article)

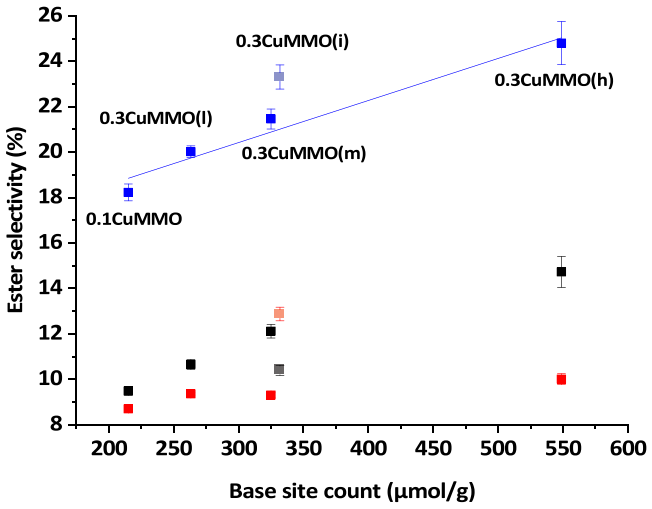

Fig. 3. Total ester selectivity (blue squares), C_{6+} ester selectivity (black squares) and ethyl acetate selectivity (red squares) vs base site count in select low-loading (0.2–0.6 wt%Cu) CuMMO catalysts. Conditions as described in Table 2. Blue line is linear fit of total ester selectivity vs base site count excluding 0.3CuMMO(i) (shown in translucent colors). Pearson's r = 0.9816, Adjusted R^2 = 0.9454. (For interpretation of the references to colour in this figure, the reader is referred to the web version of this article.)

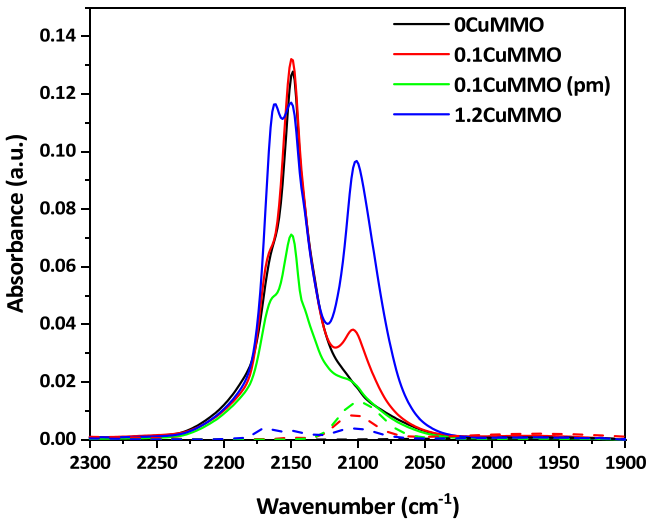

Fig. 4. IR spectra at 3 Torr of CO on 0CuMMO, 0.1CuMMO, 0.1CuMMO(pm) and 1.2CuMMO recorded at −150 °C. Solid lines represent spectra obtained after CO dosing. Dashed lines represent spectra obtained after 9 min evacuation. Catalysts were reduced *in situ* in flowing 4% H_2/N_2 at 325 °C before spectra were collected. Baselines of measurements were subtracted in the 1900–2300 cm^{-1} range so that new baseline is zero for all data.

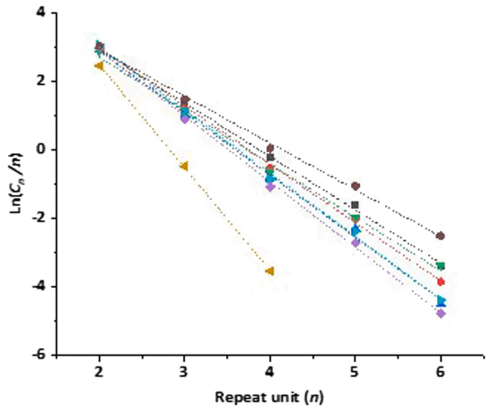

Fig. 5. Schultz-Flory distribution plots for primary alcohols for 0.3CuMMO(vl) (black squares, α = 0.210 ± 0.008), 0.3CuMMO(l) (red circles, α = 0.182 ± 0.006), 0.3CuMMO(m) (blue up triangles, α = 0.162 ± 0.009), 0.3CuMMO(h) (green down triangles, α = 0.21 ± 0.01), 0.3CuMMO(i) (purple diamonds, α = 0.147 ± 0.006), 1.2CuMMO (ochre left triangles, α = 0.050 ± 0.002), 0.1CuMMO (cyan right triangle, α = 0.158 ± 0.007) and 0.1CuMMO (pm) (brown hexagons, α = 0.26 ± 0.01). Dashed lines denote linear fits defined in Eq. (5). Conditions as described in Table 2. (For interpretation of the references to colour in this figure, the reader is referred to the web version of this article)

3. Results and discussion

3.1. Catalyst characterization and properties

The measured properties of the prepared catalysts are in Table 1. The BET surface area of the low surface area catalysts (vl and l) increased after calcination, while the BET surface area of the other materials decreased after calcination. For the low surface area materials, the increase in surface area may be explained by calcination-induced turbostractic disorder formation of the former LDH, in which the layers of the material (now-MMO) undergo small distortions after the anions and the water is removed from the layers of the material, exposing more surfaces. The reduction in area for the higher surface area materials could be explained by thermal sintering of the material, by which the layers stack up on top of each other upon calcination, reducing available surface area. The pore volume of the catalysts is proportional to the BET surface area. As shown in Figs. S1 and S2 the catalysts are almost exclusively mesoporous. As shown in Fig. 1, the concentration of base sites is proportional to the pore volume for the Cu containing catalysts, suggesting that most base sites may be located inside the pores of the catalyst due to incorporation of Cu in the materials. This positive correlation still holds if the density of base sites (µmol/m^2) is considered as shown in Fig. S4. Catalysts have varying acid site concentrations, with 0.3CuMMO(vl) having more than twice the acidity of the catalyst with next lowest acid site count (0.3CuMMO(m)), potentially because of requiring a more extensive wash to remove its higher residual Na

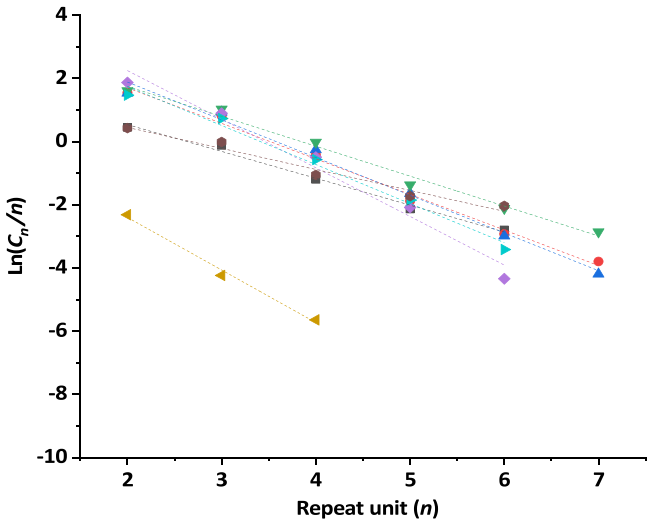

Fig. 6. Schultz-Flory distribution plots for esters for 0.3CuMMO(vl) (black squares, $\alpha = 0.43 \pm 0.02$), 0.3CuMMO(l) (red circles, $\alpha = 0.32 \pm 0.02$), 0.3CuMMO(m) (blue up triangles, $\alpha = 0.30 \pm 0.02$), 0.3CuMMO(h) (green down triangles, $\alpha = 0.39 \pm 0.02$), 0.3CuMMO(i) (purple diamonds, $\alpha = 0.21 \pm 0.03$), 1.2CuMMO (ochre left triangles, $\alpha = 0.19 \pm 0.03$), 0.1CuMMO (cyan right triangle, $\alpha = 0.29 \pm 0.02$) and 0.1CuMMO(pm) (brown hexagons, $\alpha = 0.51 \pm 0.01$). Dashed lines denote linear fits defined in Eq. (5). Conditions as described in Table 2. (For interpretation of the references to colour in this figure, the reader is referred to the web version of this article)

content compared to the other materials. Unfortunately, we were not able to measure the number of Cu active sites on the catalysts in this work due to the low loading of the Cu catalysts. Improved chemisorption techniques will be required to accurately measure the concentration of Cu metallic sites for such low Cu loading catalysts in the future.

As seen from X-ray diffractograms in Fig. S3, all calcined materials had visible peaks resembling a periclase MgO phase (PDF # 04–002–3057), indicating that the materials are solid solutions in which Al is incorporated in the MgO-like lattice of the MMO [21,30] which is reported to occur when Mg/Al ratio is > 1 [24]. The 0.3CuMMO(vl) catalyst had some visible Al_2O_3 peaks (PDF # 00–010–0425), explaining its higher acidity. The 0.3CuMMO(i) in which Cu was added via incipient wetness impregnation exhibits a peak that may be matched to CuO (PDF # 01–078–0428) at 74.0°, but its presence as crystalline nanoparticles is ambiguous given that any higher intensity peak of CuO (36.6 and 42.6°) will be masked by MgO signals. Neither Cu nor CuO were observed in the other XRD peaks, indicating that it is probably well dispersed in the MMO.

3.2. Catalyst activity and selectivities to key species in the alcohol oligomerization reaction

More than 160 products were detected after reaction. Table 2 shows the ethanol selectivity, diesel fuel precursor selectivity (DFPS), C_6 linear to branched alcohol ratios, α-values (chain growth) of alcohols and α-values of esters assuming ethanol as the monomer unit, and selectivity of major classes of products. Table S1 shows the selectivities of each of the tested catalyst to the different product categories detected, whereas the detailed product distribution per C-size over each catalyst is in Tables S2–S9. In general, the low loading catalysts (0.1–0.6 Cu wt%) exhibit high selectivity towards higher alcohols, followed by esters, then aldehydes, then ketones and other products at the same reaction conditions. 0.3CuMMO(vl), 0.3CuMMO(l), 0.3CuMMO(m) and 0.3CuMMO (h) catalysts exhibited approximately the same conversion (49 – 54%), whereas 0.3CuMMO(i), 1.2CuMMO, 0.1CuMMO and the physical mixture of 1.2CuMMO and 0CuMMO showed lower conversions (39 – 45%). The DFPS was similar for all low Cu loading catalysts, ranging between 75% and 84%. The DFPS decreased to 49% for the 1.2 CuMMO catalyst because of the higher selectivities exhibited towards smaller molecules, particularly ethyl acetate and acetone for this material. All catalysts had linear-to-branched C_6 alcohol ratios greater than 3. Ca-HAP had a linear to branched C_6 alcohol ratio of 0.8 [6]. This suggests that for the CuMMO catalysts chain growth occurs either by an increased frequency of nucleophilic attacks of an ethanol-derived intermediate to any other alcohol-derived intermediate compared to that of Ca-HAP, or by a decreased frequency of nucleophilic attacks to ethanol. Large amounts of C_{6+} esters were also observed including ethyl butyrate, butyl acetate, butyl butyrate, ethyl hexanoate, hexyl acetate, butyl hexanoate, hexyl butyrate, butyl-2-ethylbutyrate, ethyl octanoate, octyl acetate and other combinations that arise from the different linear and branched alcohols, up to C_{14} sizes. Aldehydes observed were acetaldehyde, butyraldehyde, hexanal, 2-ethylbutanal, octanal and 2-ethylhexanal. No alkenals (such as crotonaldehyde) were observed in the products, but alkenols such as crotyl alcohols were seen.

As shown in Fig. 2, alcohol selectivity varies inversely with BET surface area for the 0.3CuMMO catalysts. Base site concentration or base site density do not have a large impact on alcohol selectivity (Fig. S5). The 1.2CuMMO catalyst has a lower alcohol selectivity while having a similar base site count compared to 0.3CuMMO(h), showing that Cu loading is a more important parameter in catalyst performance than base sites. 0.3CuMMO(i) being present in the correlation indicates that the preparation method for the MMO does not impact on its own selectivity to alcohols. A monotonic increase of ester selectivity with base sites is observed for 0.2–0.4 wt%Cu loading materials as shown in Fig. 3. The ethyl acetate selectivity is very similar for these catalysts as well. The selectivity to higher esters increases monotonically with base sites for similar Cu wt% loading catalysts (0.2–0.4 wt%Cu). The 0.3CuMMO(vl) catalyst is excluded from Fig. 3 since this catalyst had at least two times higher acid site concentration than other 0.3CuMMO which caused an increase in olefin selectivity. The incipient wetness impregnation prepared 0.3CuMMO(i) catalyst is displayed in Fig. 3 but excluded from this correlation since it is observed that this material has a higher Cu content (~0.6 wt%) than the other 0.3CuMMO samples, which leads to a higher ethyl acetate selectivity. Similar observations for ester selectivity as a function of density of base sites are also observed (Fig. S6). The increase of ester formation related to base site counts can be explained by the promotion by these sites of hemiacetal species formation from alcohols and aldehydes which eventually leads to ester formation by dehydrogenation on Cu sites[14,31,32].

The 1.2CuMMO catalyst exhibited a higher ester and ketone selectivity and lower alcohol selectivity than any of the studied catalysts. These results are consistent with prior work done by our group[33], as well as the work of Ramasamy and coworkers, [18,19] and others[15,16,34] who reported that higher loading Cu catalysts are more selective to esters and ketones. Ramasamy and coworkers particularly claimed that the low loading Cu catalysts had a higher selectivity to alcohols than ethyl acetate because the Cu was in a $+1$ oxidation state, whereas higher loading Cu catalysts (≥ 0.25 wt%) had a Cu^0 oxidation state[18,19]. They observed the Cu oxidation state using XANES and EXAFS which are bulk techniques. This observation would not extend to catalyst prepared via incipient wetness impregnation[19]. However, the selectivity of a physical mixture of 1.2 CuMMO and MMO (0.1 CuMMO (pm)) is similar in selectivity to the low loading Cu catalysts, and so is the one obtained by 0.3CuMMO(i) prepared by incipient wetness impregnation (which would have Cu as Cu^0 on the surface). This indicates that Cu^0 based catalysts can also have a similar selectivity to alcohols and esters as lower loading Cu catalysts regardless of synthesis method.

We obtained FT-IR spectra of 0CuMMO, 0.1CuMMO, 0.1CuMMO (pm) and 1.2CuMMO after dosing CO at −150 °C to further study the oxidation state of Cu in these catalysts. Low temperature CO adsorption on Cu catalysts has been reported to be an accurate approach to measure the oxidation state of Cu in the catalyst surface as Cu^0 and Cu^{+1} have

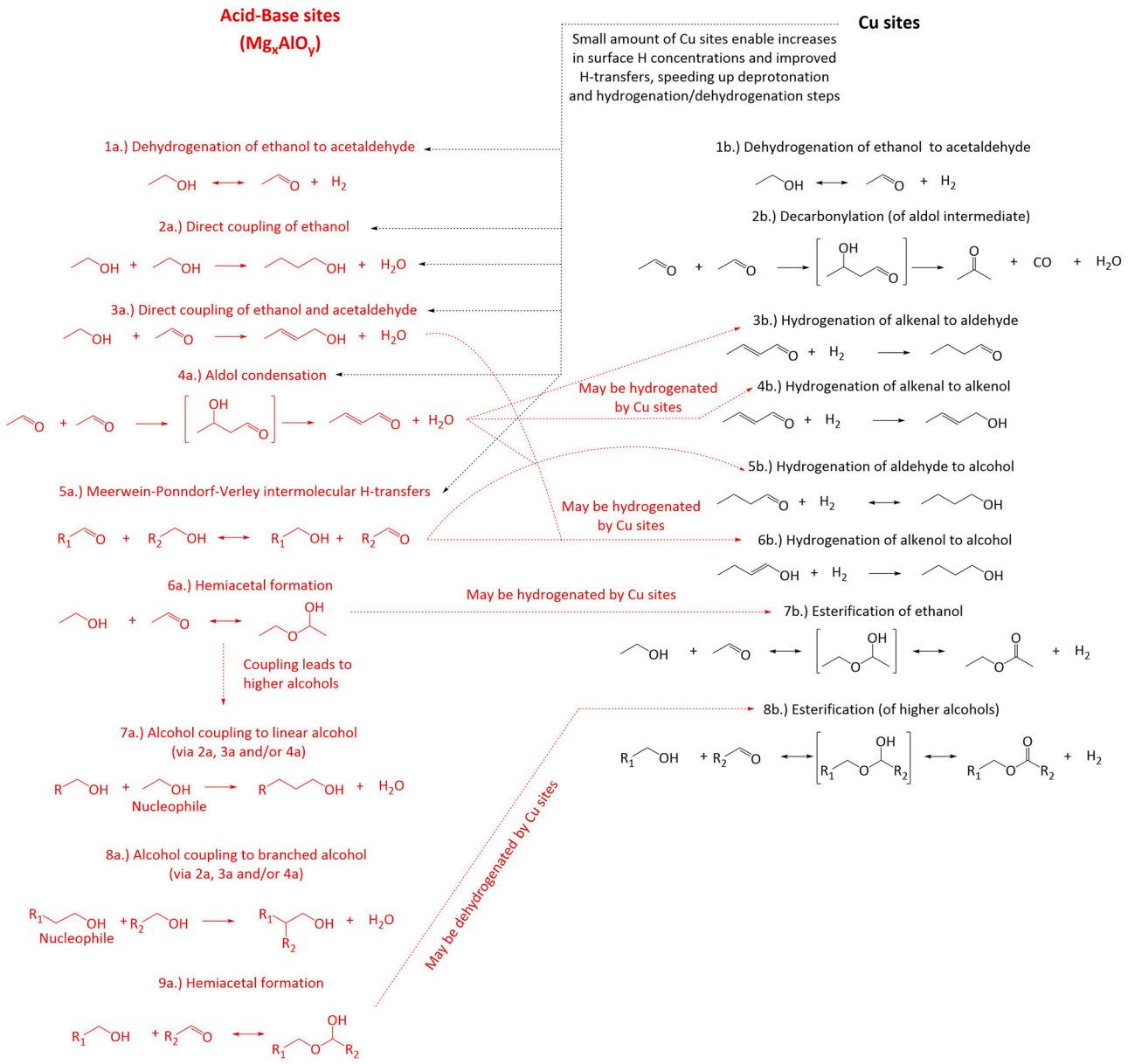

Fig. 7. List of main reactions catalyzed by Cu/Mg_xAlO_y catalysts. Main reactions catalyzed by acid-base sites are shown in red. Main reactions catalyzed by Cu sites are shown in black. Synergies between reaction steps on Cu sites and products from acid-base catalyzed steps are indicated in red dashed arrows. Synergies between reaction steps of acid-base catalyzed reactions and small amounts of Cu sites are shown in dashed black arrows. (For interpretation of the references to colour in this figure, the reader is referred to the web version of this article)

distant bands in the FTIR at 2091–2117 cm^{-1} for Cu^0 [35] and 2145–2160 cm^{-1} for Cu^{+1} [36]. The CO dosing and evacuation FT-IR spectra are shown in Fig. 4. It is observed that all materials aside from 0CuMMO show a peak at 2104 cm^{-1}, corresponding to the CO-Cu^0 band [35] indicative of Cu^0 species. There are also peaks at 2150 and 2162 cm^{-1} observed for all the analyzed materials including 0CuMMO. This indicates that these peaks come from the MgAl oxide itself rather than Cu^{+1} species. Furthermore, these two peaks completely disappear after evacuation for all but 1.2CuMMO material, in which the height of the remnant peak is 1/40th of the original peak. Since CO is known to strongly adsorb in the surface of Cu^{+1} sites [36], we would have expected that whichever peak that could correspond to Cu^{+1} (2150 or 2162 cm^{-1}) remained present after evacuation with little change. Because no peaks remained after evacuation, we can conclude that none of the catalysts analyzed exhibit Cu^{+1} sites on the surface. This observation would then apply by extension to all the materials synthesized in this work.

The peak at 2104 cm^{-1} (CO-Cu^0 band) for 0.1CuMMO, 0.1CuMMO (pm) and 1.2CuMMO was deconvoluted using a Gaussian function in order to obtain its area (please refer to Table S10 and Fig. S7). We note that the area of this peak on the 1.2CuMMO material is only 2.8 times greater than that of the 0.1CuMMO material. The former material has about 7.5 times more Cu than the latter. This indicates that the dispersion of Cu of 0.1CuMMO is much greater than that of the 1.2CuMMO, which is expected of a lower loading material. The area of the same peak of the 0.1CuMMO material in turn is about 1.7 times greater than that of the peak in the physical mixture, which is more consistent to the ratio of Cu loadings between 0.1CuMMO and 0.1CuMMO(pm) being about 1.4.

The 0.1CuMMO catalyst exhibited a similar performance to that of the 0.3CuMMO catalysts, with slightly higher alcohol selectivity and similarly lower ester selectivity. Moreover, the physical mixture experiment results show that by mixing a higher loading CuMMO material

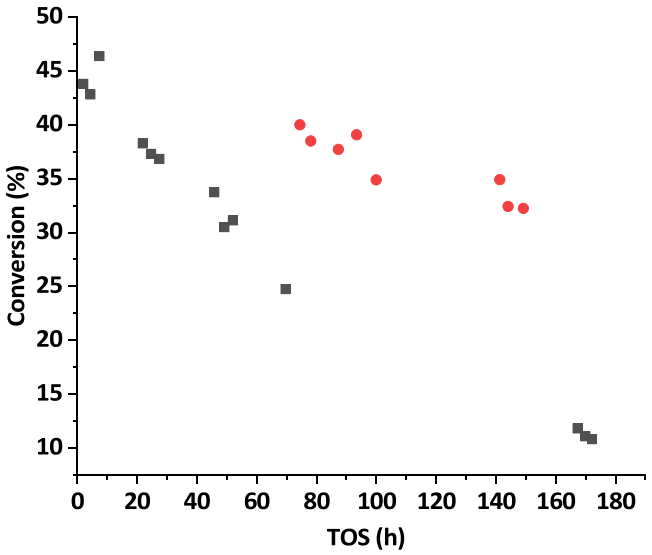

Fig. 8. Stability test of 0.1CuMMO at 6.56 h^{-1} (black squares) and 1.48 h^{-1} (red circles). Conditions: 325 °C, 300 psi, 1.00 g catalyst, p_{EtOH}:p_{H2} = 4.

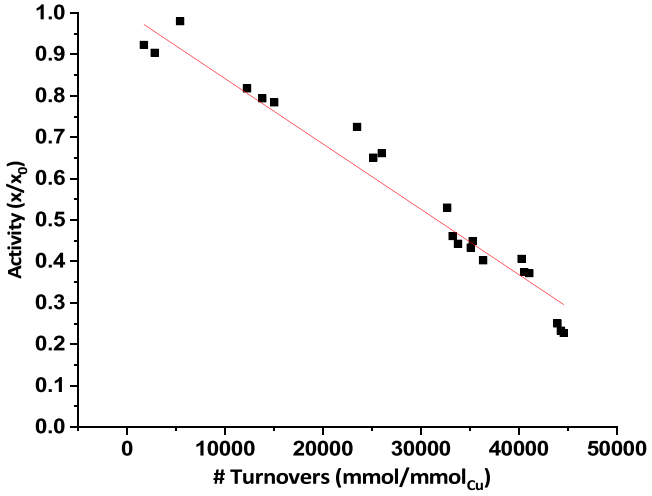

Fig. 9. Normalized activity vs turnovers for 0.1CuMMO. Conditions as in Fig. 8. Red line is fit of activity vs #Turnovers, with activity as defined by Eq. (6): $a = x/x_0 = 1 - 1.58 \times 10^{-5} T_n$, where $R^2 = 0.9939$ and slope = (1.58 ± 0.03) x 10^{-5}. (For interpretation of the references to colour in this figure, the reader is referred to the web version of this article.)

such as 1.2CuMMO with undoped calcined LDH (0CuMMO), it is possible to obtain even higher alcohol selectivities and lower ester selectivities at just a slightly lower conversion than the other CuMMO catalysts at the same conditions. The higher C_{4+} alcohol selectivity and lower C_{6+} ester selectivity obtained from the physical mixture experiment might also be the result of having less actual Cu wt% in the mixture (~0.1 wt%) than in the 0.1CuMMO catalyst (~0.2 wt%).

Overall, all of the results obtained for the different catalysts suggest that Cu has a promotional role in the rates of reaction steps that involve H-transfers, including ethanol dehydrogenation to acetaldehyde. More importantly, such H-transfer role may be accomplished by very small amounts of Cu, regardless of how Cu is added to the catalyst as shown by the similar performance between 0.3CuMMO(i) to the other 0.3CuMMO, and more remarkably, the slightly better performance of 0.1CuMMO (pm) compared to 0.1CuMMO. Once Cu is added in larger quantities, rates to side reactions proper to the Cu element such as esterification and ketone formation will become significant, resulting in lower DFP

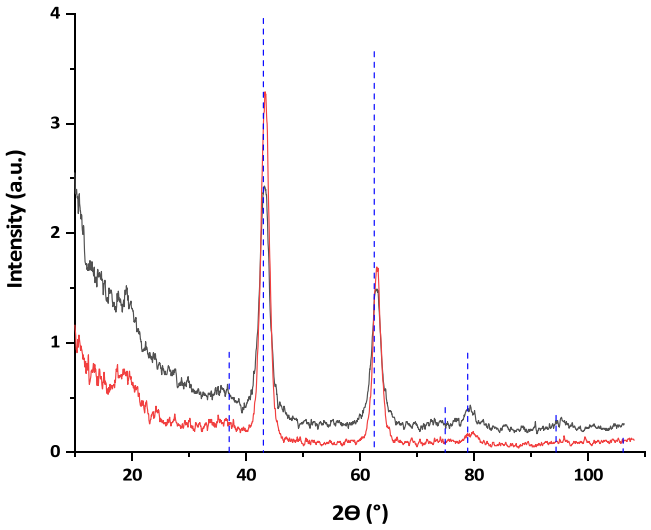

Fig. 10. Powder XRD of fresh (black) and spent (red) calcined 0.1CuMMO. Blue dashed lines represent MgO periclase peaks (PDF # 04–002–3057). X-ray source used was Cu kα (λ = 1.54 Å). (For interpretation of the references to colour in this figure, the reader is referred to the web version of this article.)

selectivity as shown by 1.2CuMMO and as reported in literature[3,14,15,33].

3.3. Schultz-Flory selectivity distributions of alcohols and esters and general reaction pathways

The alcohol selectivities fit the Schultz-Flory model (R^2 = 0.9933–0.9997) regardless of Cu loading as shown in Fig. 5. The chain growth propagation for the alcohols (α) of the 0.1 – 0.6 wt% Cu catalysts ranges from 0.147 to 0.210 with no apparent correlation to surface area, base sites counts or product selectivity. The >1.2 wt% Cu catalyst had a lower α value of 0.050, which can be related to the fact that this catalyst has lower selectivity to alcohols. The physical mixture had an α value of 0.26 which is slightly greater than the values for the 0.1–0.6 wt% Cu catalysts. This shows that chain growth occurs in all catalysts by a step growth mechanism and that electrophilicity of all alcohols is similar regardless of the alcohol size as per the distribution model assumption in which all chains have the same reactivity as described by the model[29] and other authors[11]. Only linear alcohols can continue acting as nucleophiles to form higher alcohols. α-branched alcohols are unable to act as nucleophiles as shown by Eagan et al.[6,12]. Moreover, in the present work we did not observe any alcohol that could be formed from the attack of a linear alcohol to an α-branched alcohol. This could be explained by steric effects on the region close to the C-O bond preventing C-C bonding to occur. This result and that of the C_6 linear:branched alcohol ratio being greater than 1 allows us to therefore conclude that CuMMO catalysts promote coupling by increasing the relative nucleophilicity (i.e. tendency to attack and form C-C bonds) of ethanol with respect to other alcohols.

Ester products also fit the Schultz-Flory distribution chain growth model as shown in Fig. 6. Their degree of fit is lower than that of the alcohol selectivities (R^2 = 0.9606 – 0.9902). The α-value for 0.1–0.6 wt % Cu-doped materials varies widely between 0.29 and 0.43, again with no apparent correlation to any property as was the case for alcohols. The α-value for the 1.2CuMMO catalyst is 0.19, which is closer to the obtained for the 0.3CuMMO(i) made by incipient wetness impregnation of 0.21. The α-value for the physical mixture is 0.51, being the largest among all materials. This may be explained if an alcohol-to-ester series mechanism is taking place as it is reported in literature for Cu-containing MMO[15,31], which can be assumed to be the case since hemiacetals (particularly 1-ethoxyethanol) were observed in the products. The larger

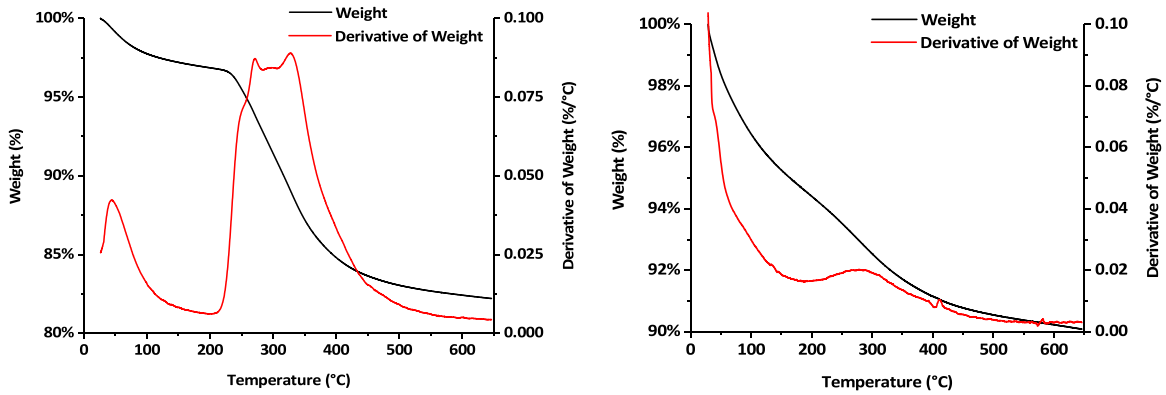

Fig. 11. TGA of 0.1CuMMO spent (left) and fresh calcined (right). TGA conditions: 25–650 °C (10 °C/min). 50 mL/min O_2, 10–15 mg sample.

esters could also be produced by transesterification reactions, in which a part of the alcohol moiety of the ester may be substituted by another one. Also, ester selectivity following Schultz-Flory distribution may indicate that the electrophilicity of aldehydes to form C-O bonds is similar regardless of their size.

To further understand the reasons behind the favorable selectivity of low Cu-loading catalysts towards diesel fuel precursors, particularly towards C_{4+} alcohols, we need to consider the contribution of each type of site in the catalysts towards the most important reactions occurring. In Fig. 7 we outline the most important reactions that happen on the Cu sites and the acid-base sites of Mg_xAlO_y. Ethanol dehydrogenation to acetaldehyde can be catalyzed by both acid-base sites (1a)[8,24,25,34], and Cu sites (1b)[15,34,37]. Alcohol condensation either via direct condensation (2a and 3a for ethanol) mechanisms, Aldol condensation (4a) or a combination of both mechanisms [38] may be catalyzed mostly by acid-base sites [24,25,34,37,39,40] of Mg_xAlO_y, in which H-transfer steps occur through intermolecular exchanges via Meerwein–Ponndorf–Verley (MPV) mechanisms (5a) that are equilibrium-limited. Cu sites catalyze decarbonylation of the aldol intermediate to a ketone (2b for acetone)[34,41]. However, Cu sites enable an increase of the concentration of surface H and allows transport of such species across the catalyst surface. This H-transfer capabilities to the material allows for H removal in deprotonation steps by forming gas phase H_2. The addition of Cu can thus increase rates of deprotonation of the β-C of ethanol and α-C of acetaldehyde (involved in steps of 2a-4a). The increased surface H concentration also increases rates of hydrogenation/dehydrogenation reactions from which the larger alcohols are increased (via 3b-6b rather than 5a). Such H-transfer reactions are reported to be the rate-limiting step of higher alcohol formation [39,42,43]. The kinetic model for ethanol coupling based on Aldol condensation developed by our group with Ca-HAP in prior work assumes deprotonation of the α-C of acetaldehyde as the rate-limiting step[12]. The low loading (0.2–0.6 wt%Cu) catalysts in this work have high C_{4+} alcohol selectivity (49 – 56%) likely because surface H can be quickly removed from deprotonation steps when Cu is added to the Mg_xAlO_y. The concentration of surface hydrogen can be increased by raising total pressure allowing for more facile hydrogenation of alcohol coupling intermediates (note that $p_{ethanol}>p_{H2}$ to boost H_2 formation from surface H via favorable equilibrium in ethanol deprotonation steps to obtain high conversion). It is remarkable then that only a very small amount of Cu is required for this to occur.

It can be concluded that Cu does not need to be atomically close to acid-base sites for two main reasons: 1)The performance of the physical mixture of 1.2CuMMO and 0CuMMO is similar to that of low Cu loading catalysts and 2) the low temperature CO adsorption experiments show that the 1.2CuMMO and 0.1CuMMO (and by extension the 0.3CuMMO) catalysts have similar types of Cu sites. The product selectivity may be expressed as a combination of the rates by each type of site separately. The higher alcohol selectivity for low Cu loading catalysts is then due to the rates of acid-base catalyzed alcohol coupling being greater than those of Cu-catalyzed esterification and ketone formation [34,37,41,44]. If Cu loadings are further increased, decarbonylation (2b) and esterification (7b, 8b) will increase and product selectivity shifts towards ketones and lighter esters (7b particularly).

Finally, another unexpected effect of having low Cu loadings in the catalysts is that since higher alcohol formation is favored (7a, 8a), it is possible to form higher esters in relatively high selectivity compared to ethyl acetate, since the higher alcohols and aldehydes would form these via formation of hemiacetals (9a rather than 6a) that can subsequently be hydrogenated by Cu sites, which are also capable on their own to fully form the higher esters (8b).

3.4. Catalyst stability and deactivation mechanism

All catalysts were observed to undergo deactivation. Fig. 8 shows the conversion of 0.1CuMMO over 170 h at two different WHSV. It can be observed that at 6.56 h^{-1} deactivation seems to be proceeding faster than at 1.48 h^{-1} (for species selectivities changes over time please refer to Fig. S8). Therefore, we decided to compare loss of activity over number of turnovers in Cu loading base to obtain a normalized way of measuring deactivation since it seems to be the most influencing parameter in catalyst selectivity. Activity is defined as the ratio of conversion at a given TOS to the initial conversion as defined by Eq. (6). Fig. 9 shows the catalyst activity as a function of turnovers for 0.1CuMMO. It can be observed that deactivation is proportional to the number of turnovers. This trend was observed for the other 0.3CuMMO catalysts as shown in Figs. S9 to S13 for select catalysts.

Deactivation of these catalysts has been reported to occur via oligomerization of aldehyde species[15], at least when no metal is incorporated. It is also possible that olefins may also undergo oligomerization in the acid sites of the catalyst and generate coke. Water generated in the alcohol coupling and dehydration reactions may rehydrate the LDH structure, promoting deactivation. X-ray diffractograms of the spent 0.1CuMMO catalyst compared to the fresh calcined material are shown in Fig. 10. The X-ray diffraction pattern of the spent catalyst compared to the fresh sample shows that the crystalline structure of the fresh and spent material correspond to the MgO-like phase expected from a solid solution of MgO and Al_2O_3 with Mg/Al > 1 [24], which allows us to conclude that no rehydration occurred. However, we do note that a ~15% decrease on peak width occurred in the spent material compared to the fresh suggesting increase of crystallite sizes. Thermogravimetric analysis (TGA) of the spent and fresh 0.1CuMMO is shown in Fig. 11. TGA shows that about 18% of the mass of the catalyst was lost when it was heated from room temperature to 650 °C. It can be observed that from 200° to 400°C, a major part of the mass loss occurs, which is consistent with loss of carbon species on the surface of the catalyst, whereas the loss that occurs at lower temperatures can be attributed mostly to water, as the fresh sample TGA shows a major mass loss only

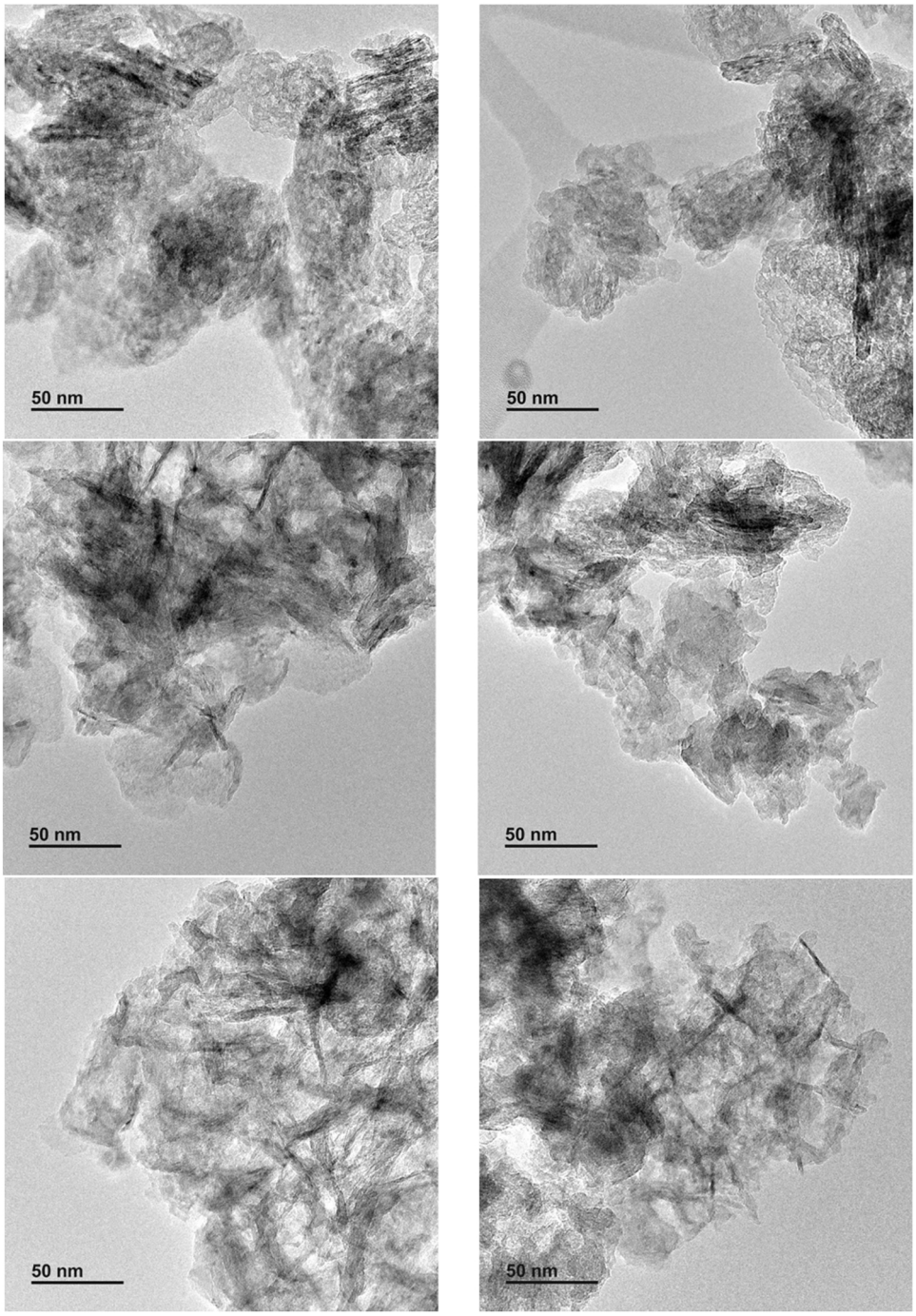

Fig. 12. TEM micrographs of 0.1CuMMO (upper), 0.3CuMMO(m) (middle) and 1.2CuMMO(lower). Micrographs to the left are of freshly calcined catalysts (600 °C, 2 h, 4 °C/min, static air). Micrographs to the right are of reduced (50 mL/min H_2, 325 °C, 1.33 h) then passivated (1% O_2/Ar pulses) catalysts.

before 200 °C. An additional confirmation of the observations made above was done by analyzing the 0.3CuMMO(m) spent sample. The results are shown in Figs. S14 and S15, where a comparison between the fresh and spent samples of 0.3CuMMO(m) catalyst is done, corroborating the results for the 0.1CuMMO material. A final piece of evidence was obtained by performing TOC analysis to the 0.1CuMMO and 0.3CuMMO(m) samples, showing that 13% and 14% of each sample mass respectively was carbon versus 1% and 2% of each fresh sample, which is consistent with deactivation via coking. We also carried out quantification of metal content analysis of select product samples by ICP-OES, and all the analyses showed no leaching of the metals into the products (i.e. metal content no different from baseline).

Another possible deactivation mechanism that occurs with metal particles is sintering. To verify if sintering is occurring, several micrographs of freshly calcined catalysts were taken and compared to micrographs of catalysts reduced at reaction conditions and then passivated with 1 O_2/Ar pulses to determine whether metal aggregation occurred. A comparison between fresh calcined and reduced and passivated images of 0.1CuMMO, 0.3CuMMO(m) and 1.2CuMMO is shown in Fig. 12. Larger areas of darker domains are observed in the reduced and passivated samples compared to the fresh materials, suggesting particle aggregation occurs. Coupling this observation to that of the decrease of peak width from the XRD analysis, we conclude that sintering is a possible deactivation mechanism. Sintering of Cu

nanoparticles has been observed on similar catalysts with higher Cu loadings for the catalytic upgrading of glycerol [45–47] and sugar fractions, with minimal decrease in activity even after 100 h TOS[45]. The same observations hold for the rest of catalysts, as shown in Fig. S16.

Finally, we regenerated 0.1CuMMO catalyst as described at the end of the Ethanol Oligomerization Reactions section. The results of the run with the regenerated catalyst compared to the fresh one is shown in Table 2 (0.1 (r) entry) and Table S1. Overall, reaction performance is very similar between fresh and regenerated batches, with the regenerated batch producing a small amount of aromatic species. Therefore, it can be concluded that the catalyst is regenerable and that the primary mechanism of deactivation within the timeframe studied is coking.

4. Conclusions

Low (0.1–0.6 wt%) Cu loadings catalysts supported on Mg_xAlO_y promote coupling of ethanol to higher predominately linear alcohols and aldehydes with high selectivity regardless of how the Cu is added to the catalyst. The low Cu catalysts exhibited high selectivities (75–84%) to diesel-fuel precursors. C_{6+} esters are another product of this reaction. The esters are combinations of the several mostly linear alcohols produced and can potentially be used as diesel fuel additives. Varying surface area of the catalyst changes the pore volume and base site counts but does not have a large impact on catalyst performance. In contrast, higher loading of Cu (>1.2 wt%) on Mg_xAlO_y produces higher amounts of ethyl acetate and ketones, significantly reducing selectivity to diesel-fuel precursor compounds. Increasing the acidity of the catalyst increases the olefin yield at the expense of ester yields.

By adding small Cu amounts to Mg_xAlO_y catalysts, the materials become able to promote higher alcohol coupling by facilitating H-transfers on the catalyst surface and enabling H_2 scission and proton recombination, accelerating acid-base-catalyzed deprotonation and hydrogenation/dehydrogenation reaction steps that would be carried out via equilibrated MPV mechanisms otherwise. Alcohol coupling then involves ethanol coupling to 1-butanol either via aldol condensation or direct condensation. 1-butanol is attacked by an ethanol-derived active species to form 1-hexanol, and a similar process occurs with any combination of alcohols in which the ethanol-derived species performs the nucleophilic attack to form increasingly larger alcohols. In any other case, primary branched alcohols are formed, and these are incapable of undergoing coupling in an appreciable manner. Ethanol may also dehydrogenate to acetaldehyde, which in turn can participate in the coupling reaction to higher alcohols depending on the mechanism, and also participates in the formation of esters such as ethyl acetate by forming C-O bonds with alcohols. Esters are formed from alcohols and aldehydes produced via hemiacetal-based mechanisms that can be catalyzed by Cu sites, and may be further helped by acid-base sites. Additional reactions include decarbonylation that gives rise to ketones, unimolecular dehydration to olefins and bimolecular dehydration to ethers.

The alcohols and esters follow a Schultz-Flory distribution chain growth model. The alcohol and ester molecules have similar electrophilicities, therefore the driving force of alcohol growth is an increased nucleophilicity of ethanol relative to the other alcohols when Cu/Mg_xAlO_y catalysts are used.

The studied catalysts deactivated proportional to the number of turnovers mainly by coking. Deactivation was reversible and the catalyst activity can be recovered by calcination.

CRediT authorship contribution statement

Paolo Cuello Penaloza: Conceptualization, Methodology, Validation, Formal analysis, Investigation, Writing – original draft, Visualization. **Raka G. Dastidar:** Investigation. **Shao-Chun Wang:** Investigation. **Yi Du:** Investigation, Writing – review & editing. **Michael P. Lanci:** Resources, Project administration. **Bradley Wooler:** Investigation. **Christine E. Kliewer:** Investigation. **Ive Hermans:** Resources. **James A. Dumesic:** Writing – review & editing. **George W. Huber:** Writing – review & editing, Resources, Project administration, Funding acquisition.

Acknowledgements

This work was supported and financed by ExxonMobil Research and Engineering Company, USA.

Conflicts of interest

The authors have no conflicts of interest to declare.

Appendix A. Supporting information

Supplementary data associated with this article can be found in the online version at doi:10.1016/j.apcatb.2021.120984.

References

[1] Exxon Mobil Corporation, 2019 Outlook for Energy: A Perspective to 2040, (n.d.). ⟨https://corporate.exxonmobil.com/-/media/Global/Files/outlook-for-energy/2019-Outlook-for-Energy_⟩v4.pdf (Accessed 19 April 2021).
[2] FedCenter - EO 13693 (Archive) - revoked by EO 13834 on May 17, 2018, Sec. 8, (n.d.). ⟨https://www.fedcenter.gov/programs/eo13693/⟩ (Accessed 19 April 2021).
[3] N.M. Eagan, M.D. Kumbhalkar, J.S. Buchanan, J.A. Dumesic, G.W. Huber, Chemistries and processes for the conversion of ethanol into middle-distillate fuels, Nat. Rev. Chem. 3 (2019) 223–249, https://doi.org/10.1038/s41570-019-0084-4.
[4] USDA Study Shows Significant Greenhouse Gas Benefits of Ethanol Compared with Gasoline, (n.d.). ⟨https://www.usda.gov/media/press-releases/2019/04/02/usda-study-shows-significant-greenhouse-gas-benefits-ethanol⟩ (Accessed 19 April 2021).
[5] G. Zang, P. Sun, A. Elgowainy, A. Bafana, M. Wang, Life cycle analysis of electrofuels: fischer–tropsch fuel production from hydrogen and corn ethanol byproduct CO_2, Environ. Sci. Technol. 55 (2021) 3888–3897, https://doi.org/10.1021/acs.est.0c05893.
[6] N.M. Eagan, B.M. Moore, D.J. McClelland, A.M. Wittrig, E. Canales, M.P. Lanci, G. W. Huber, Catalytic synthesis of distillate-range ethers and olefins from ethanol through Guerbet coupling and etherification, Green Chem. 21 (2019) 3300–3318, https://doi.org/10.1039/C9GC01290G.
[7] N.A. Huq, X. Huo, G.R. Hafenstine, S.M. Tifft, J. Stunkel, E.D. Christensen, G. M. Fioroni, L. Fouts, R.L. McCormick, P.A. Cherry, C.S. McEnally, L.D. Pfefferle, M. R. Wiatrowski, P.T. Benavides, M.J. Biddy, R.M. Connatser, M.D. Kass, T. L. Alleman, P.C.S. John, S. Kim, D.R. Vardon, Performance-advantaged ether diesel bioblendstock production by a priori design, Proc. Natl. Acad. Sci. 116 (2019) 26421–26430, https://doi.org/10.1073/pnas.1911107116.
[8] J.T. Kozlowski, R.J. Davis, Heterogeneous catalysts for the guerbet coupling of alcohols, ACS Catal. 3 (2013) 1588–1600, https://doi.org/10.1021/cs400292f.
[9] L. Silvester, J.-F. Lamonier, C. Lamonier, M. Capron, R.-N. Vannier, A.-S. Mamede, F. Dumeignil, Guerbet reaction over strontium-substituted hydroxyapatite catalysts prepared at various (Ca+Sr)/P ratios, ChemCatChem 9 (2017) 2250–2261, https://doi.org/10.1002/cctc.201601480.
[10] S. Hanspal, Z.D. Young, J.T. Prillaman, R.J. Davis, Influence of surface acid and base sites on the Guerbet coupling of ethanol to butanol over metal phosphate catalysts, J. Catal. 352 (2017) 182–190, https://doi.org/10.1016/j.jcat.2017.04.036.
[11] T. Moteki, D.W. Flaherty, Mechanistic insight to C—C bond formation and predictive models for cascade reactions among alcohols on Ca- and Sr-hydroxyapatites, ACS Catal. 6 (2016) 4170–4183, https://doi.org/10.1021/acscatal.6b00556.
[12] N.M. Eagan, M.P. Lanci, G.W. Huber, Kinetic modeling of alcohol oligomerization over calcium hydroxyapatite, ACS Catal. 10 (2020) 2978–2989, https://doi.org/10.1021/acscatal.9b04734.
[13] M. De Bruyn, Z. Sun, K. Barta, Chapter three - the thousand faces of Cu-doped porous mixed oxides (Cu-PMO) in the conversion of renewable resources and beyond, in: P.C. Ford, R. van Eldik (Eds.), Advances in Inorganic Chemistry, Academic Press, 2021, pp. 59–98, https://doi.org/10.1016/bs.adioch.2020.12.002.
[14] I.-C. Marcu, D. Tichit, F. Fajula, N. Tanchoux, Catalytic valorization of bioethanol over Cu-Mg-Al mixed oxide catalysts, Catal. Today 147 (2009) 231–238, https://doi.org/10.1016/j.cattod.2009.04.004.
[15] J.J. Bravo-Suárez, B. Subramaniam, R.V. Chaudhari, Vapor-phase methanol and ethanol coupling reactions on CuMgAl mixed metal oxides, Appl. Catal. Gen. 455 (2013) 234–246, https://doi.org/10.1016/j.apcata.2013.01.025.
[16] F. Cheng, H. Guo, J. Cui, B. Hou, D. Li, Guerbet reaction of methanol and ethanol catalyzed by CuMgAlOx mixed oxides: effect of M2+/Al3+ ratio, J. Fuel Chem. Technol. 46 (2018) 1472–1481, https://doi.org/10.1016/S1872-5813(18)30061-6.

[17] H.M. Job, M. J. Gray, and K. K. Ramasamy. "Reaction Mechanism Studies of Ethanol Coupling over Mixed Oxide Catalyst." Presented at the Symposium on Thermal and Catalytic Sciences for Biofuels and Biobased Products, Chapel Hill, North Carolina, United States 2016.
[18] M.J. Gray, C. Alvarez-Vasco, M. Guo and K. K. Ramasamy. "Distillate Generation via Guerbet Alcohol Coupling from Biomass." Presented at the Symposium on Thermal and Catalytic Sciences for Biofuels and Biobased Products, Chapel Hill, North Carolina, United States 2016.
[19] K.K. Ramasamy, M.F. Guo, M.J. Gray, S. Subramaniam, United States Patent: 10745330 - method of converting ethanol to higher alcohols, 10745330, 2020. ⟨http://patft.uspto.gov/netacgi/nph-Parser?Sect1=PTO1&Sect2=HITOFF&d=PALL&p=1&u=%2Fnetahtml%2FPTO%2Fsrchnum.htm&r=1&f=G&l=50&s1=10,⟩745⟨,330.PN.&OS=PN/10,⟩745⟨,330&RS=PN/10,⟩745⟨,330⟩ (accessed August 30, 2020).
[20] K.K. Ramasamy, M. Gray, H. Job, C. Smith, Y. Wang, Tunable catalytic properties of bi-functional mixed oxides in ethanol conversion to high value compounds, Catal. Today 269 (2016) 82–87, https://doi.org/10.1016/j.cattod.2015.11.045.
[21] K.K. Ramasamy, M. Gray, H. Job, D. Santosa, X.S. Li, A. Devaraj, A. Karkamkar, Y. Wang, Role of calcination temperature on the hydrotalcite derived MgO–Al2O3 in converting ethanol to butanol, Top. Catal. 59 (2016) 46–54, https://doi.org/10.1007/s11244-015-0504-8.
[22] C. Chen, M. Yang, Q. Wang, J.-C. Buffet, D. O'Hare, Synthesis and characterisation of aqueous miscible organic-layered double hydroxides, J. Mater. Chem. A 2 (2014) 15102–15110, https://doi.org/10.1039/C4TA02277G.
[23] Q. Wang, D. O'Hare, Large-scale synthesis of highly dispersed layered double hydroxide powders containing delaminated single layer nanosheets, Chem. Commun. 49 (2013) 6301–6303, https://doi.org/10.1039/C3CC42918K.
[24] V.K. Díez, C.R. Apesteguía, J.I. Di Cosimo, Effect of the chemical composition on the catalytic performance of MgyAlOx catalysts for alcohol elimination reactions, J. Catal. 215 (2003) 220–233, https://doi.org/10.1016/S0021-9517(03)00010-1.
[25] J.I. Di Cosimo, C.R. Apesteguı&ca, M.J.L. Ginés, E. Iglesia, Structural requirements and reaction pathways in condensation reactions of alcohols on MgyAlOx catalysts, J. Catal. 190 (2000) 261–275, https://doi.org/10.1006/jcat.1999.2734.
[26] J.I. Di Cosimo, V.K. Díez, M. Xu, E. Iglesia, C.R. Apesteguía, Structure and surface and catalytic properties of Mg-Al basic oxides, J. Catal. 178 (1998) 499–510, https://doi.org/10.1006/jcat.1998.2161.
[27] P.H. Galebach, D.J. McClelland, N.M. Eagan, A.M. Wittrig, J.S. Buchanan, J. A. Dumesic, G.W. Huber, Production of alcohols from cellulose by supercritical methanol depolymerization and hydrodeoxygenation, ACS Sustain. Chem. Eng. 6 (2018) 4330–4344, https://doi.org/10.1021/acssuschemeng.7b04820.
[28] D. Takeuchi, K. Osakada, Oligomerization of olefins, in: K. Osakada (Ed.), Organomet. React. Polym, Springer, Berlin, Heidelberg, 2014, pp. 169–215, https://doi.org/10.1007/978-3-662-43539-7_5.
[29] C.T. Young, R. von Goetze, A.K. Tomov, F. Zaccaria, G.J.P. Britovsek, The mathematics of ethylene oligomerisation and polymerisation, Top. Catal. 63 (2020) 294–318, https://doi.org/10.1007/s11244-019-01210-0.
[30] P. Kuśtrowski, L. Chmielarz, E. Bożek, M. Sawalha, F. Roessner, Acidity and basicity of hydrotalcite derived mixed Mg–Al oxides studied by test reaction of MBOH conversion and temperature programmed desorption of NH3 and CO_2, Mater. Res. Bull. 39 (2004) 263–281, https://doi.org/10.1016/j.materresbull.2003.09.032.
[31] K. Inui, T. Kurabayashi, S. Sato, Direct synthesis of ethyl acetate from ethanol carried out under pressure, J. Catal. 212 (2002) 207–215, https://doi.org/10.1006/jcat.2002.3769.
[32] M. Hronec, K. Fulajtárová, B. Horváth, T. Liptaj, E. Dobročka, A facile conversion of furfural to novel tetrahydrofurfuryl hemiacetals, Appl. Catal. Gen. 594 (2020), 117471, https://doi.org/10.1016/j.apcata.2020.117471.
[33] D.D. Petrolini, N. Eagan, M.R. Ball, S.P. Burt, I. Hermans, G.W. Huber, J. A. Dumesic, L. Martins, Ethanol condensation at elevated pressure over copper on AlMgO and AlCaO porous mixed-oxide supports, Catal. Sci. Technol. 9 (2019) 2032–2042, https://doi.org/10.1039/C9CY00316A.
[34] E. Iglesia, D.G. Barton, J.A. Biscardi, M.J.L. Gines, S.L. Soled, Bifunctional pathways in catalysis by solid acids and bases, Catal. Today 38 (1997) 339–360, https://doi.org/10.1016/S0920-5861(97)81503-7.
[35] I. Ro, Y. Liu, M.R. Ball, D.H.K. Jackson, J.P. Chada, C. Sener, T.F. Kuech, R. J. Madon, G.W. Huber, J.A. Dumesic, Role of the Cu-ZrO2 interfacial sites for conversion of ethanol to ethyl acetate and synthesis of methanol from CO_2 and H2, ACS Catal. 6 (2016) 7040–7050, https://doi.org/10.1021/acscatal.6b01805.
[36] G.D. Borgard, S. Molvik, P. Balaraman, T.W. Root, J.A. Dumesic, Microcalorimetric and infrared spectroscopic studies of CO, C2H4, N2O, and O2 adsorption on Cu-Y zeolite, Langmuir 11 (1995) 2065–2070, https://doi.org/10.1021/la00006a037.
[37] M.J.L. Gines, E. Iglesia, Bifunctional condensation reactions of alcohols on basic oxides modified by copper and potassium, J. Catal. 176 (1998) 155–172, https://doi.org/10.1006/jcat.1998.2009.
[38] E.F. de Souza, H.P. Pacheco, N. Miyake, R.J. Davis, F.S. Toniolo, Computational and experimental mechanistic insights into the ethanol-to-butanol upgrading reaction over MgO, ACS Catal. 10 (2020) 15162–15177, https://doi.org/10.1021/acscatal.0c04616.
[39] F.C. Meunier, J. Scalbert, F. Thibault-Starzyk, Unraveling the mechanism of catalytic reactions through combined kinetic and thermodynamic analyses: application to the condensation of ethanol, Comptes Rendus Chim. 18 (2015) 345–350, https://doi.org/10.1016/j.crci.2014.07.002.
[40] A.S. Ndou, N. Plint, N.J. Coville, Dimerisation of ethanol to butanol over solid-base catalysts, Appl. Catal. Gen. 251 (2003) 337–345, https://doi.org/10.1016/S0926-860X(03)00363-6.
[41] M. Neurock, Z. Tao, A. Chemburkar, D.D. Hibbitts, E. Iglesia, Theoretical insights into the sites and mechanisms for base catalyzed esterification and aldol condensation reactions over Cu, Faraday Discuss. 197 (2017) 59–86, https://doi.org/10.1039/C6FD00226A.
[42] J. Pang, M. Zheng, L. He, L. Li, X. Pan, A. Wang, X. Wang, T. Zhang, Upgrading ethanol to n-butanol over highly dispersed Ni–MgAlO catalysts, J. Catal. 344 (2016) 184–193, https://doi.org/10.1016/j.jcat.2016.08.024.
[43] S. Ogo, A. Onda, Y. Iwasa, K. Hara, A. Fukuoka, K. Yanagisawa, 1-Butanol synthesis from ethanol over strontium phosphate hydroxyapatite catalysts with various Sr/P ratios, J. Catal. 296 (2012) 24–30, https://doi.org/10.1016/j.jcat.2012.08.019.
[44] M.E. Sad, M. Neurock, E. Iglesia, Formation of C–C and C–O bonds and oxygen removal in reactions of alkanediols, alkanols, and alkanals on copper catalysts, J. Am. Chem. Soc. 133 (2011) 20384–20398, https://doi.org/10.1021/ja207551f.
[45] P.H. Galebach, J.K. Soeherman, A.M. Wittrig, M.P. Lanci, G.W. Huber, Supercritical methanol depolymerization and hydrodeoxygenation of maple wood and biomass-derived oxygenates into renewable alcohols in a continuous flow reactor, ACS Sustain. Chem. Eng. 7 (2019) 15361–15372, https://doi.org/10.1021/acssuschemeng.9b02704.
[46] P.H. Galebach, M. Beussman, J. Johnson, T. Fredriksen, C. Wang, M.P. Lanci, G. W. Huber, Catalytic conversion of pyrolysis oil to alcohols and alkanes in supercritical methanol over the CuMgAlOx catalyst, ACS Sustain. Chem. Eng. 9 (2021) 2067–2079, https://doi.org/10.1021/acssuschemeng.0c07020.
[47] W. Yin, R.H. Venderbosch, G. Bottari, K.K. Krawzcyk, K. Barta, H.J. Heeres, Catalytic upgrading of sugar fractions from pyrolysis oils in supercritical mono-alcohols over Cu doped porous metal oxide, Appl. Catal. B Environ. 166–167 (2015) 56–65, https://doi.org/10.1016/j.apcatb.2014.10.065.